RESEARCH ARTICLE | FEBRUARY 06 2025

Combined effects of Hall and ion-slip currents and heat transfer on peristaltic transport of a copper–water nanofluid

Khalid Nowar ; Borhen Halouani

AIP Advances 15, 025307 (2025)
https://doi.org/10.1063/5.0246334

Combined effects of Hall and ion-slip currents and heat transfer on peristaltic transport of a copper–water nanofluid

Cite as: AIP Advances 15, 025307 (2025); doi: 10.1063/5.0246334
Submitted: 31 October 2024 • Accepted: 27 January 2025 •
Published Online: 6 February 2025

Khalid Nowar[a) and Borhen Halouani[b)

AFFILIATIONS

Department of Mathematics, College of Sciences, King Saud University, P.O. Box 2455, Riyadh 11451, Saudi Arabia

[a)]**Email:** khnowar@ksu.edu.sa
[b)]**Author to whom correspondence should be addressed:** halouani@ksu.edu.sa

ABSTRACT

This work has looked at theoretically the peristaltic transport of copper–water nanofluid across an asymmetric horizontal channel with a constant applied magnetic field. Heat transfer and Hall and ion-slip currents are also taken into account. Long wave length and low Reynolds number are presumptions used in mathematical modeling. Exact analytic solutions for the present model are obtained. The expressions for the velocity field, stream function, pressure gradient, pressure rise, temperature distribution, and nanoparticle concentration are computed. The trapping phenomena have been also discussed. Graphics were used in the research to demonstrate how various factors impact the flow quantities of interest. According to the results, raising the Hall parameter or adding copper nanoparticles causes the base fluid velocity to increase at the channel's center while decreasing toward the channel's walls. Furthermore, it was found that, by increasing the magnitude of nanoparticle volume fraction or by adding copper nanoparticles, the Hall parameter has a diminishing influence on the pressure gradient, as well as on the temperature of the base fluid. In addition, the number of trapped boluses increases in the upper half of the channel as the Hall parameter, the volume fraction of nanoparticles, or the Grashof number increases. Exploring the combined effects of heat transfer, Hall and ion-slip currents, and peristaltic transport of a copper–water nanofluid is important for expanding our knowledge of basic science concepts related to fluid dynamics and heat transfer, as well as for real-world engineering and technological applications.

I. INTRODUCTION

Nanofluids are a type of fluid having nanometer-sized particles known as nanoparticles (having sizes less than 10^{-2}). Colloidal nanoparticle suspensions in base fluids are what these fluids are made of. Typically, metals, oxides, carbides, nitrides, or nonmetals such as graphite or carbon nanotubes are utilized to make the nanoparticles used in nanofluids. Oil, water, and ethylene glycol are examples of common base fluids. Researchers are increasingly interested in the flow analysis of nanofluids due to their new features, which might make them helpful in a variety of applications such as heat transfer, microelectronics, fuel cells, pharmaceutical procedures, and hybrid engines. Nanofluids are utilized extensively in engineering, medicine, and electrical devices, including modern drug-delivery systems, improved systems for cooling and heating, electronic device batteries, cooling fluids in nuclear reactors, motor vehicles, industrial cooling, geothermal energy extraction, medical diagnostics, hyperthermia, cancer therapy, and cryosurgery. Due to such variants and useful applications, several theoretical and experimental investigations were carried out to analyze different aspects of nanofluids (see Refs. 1–12).

Recently, the magnetohydrodynamic (MHD) peristaltic flow of electrically conducting fluids has received great attention from many researchers.[13–22] This is because it has a variety of uses in bioengineering and medical sciences. The MHD characteristics are useful in understanding some practical phenomena such as blood pump machines; magnetic resonance imaging (MRI), which is used for diagnosis of brain; cancer tumor treatment; vascular diseases; hyperthermia; and blood reduction during surgeries. Furthermore, the study of MHD flows with Hall currents has important engineering applications in problems of magnetohydrodynamic generators and Hall accelerators, as well as in flight magnetohydrodynamics. In fact, the Hall effect is significant when the Hall parameter is high. This happens when the magnetic field is strong. The Hall current arises from the interaction between electric and magnetic fields in a conducting medium, resulting in a transverse current, while the ion-slip current refers to the current generated due to the relative motion between ions and electrons in a plasma flowing through a magnetic field. Both phenomena are important in understanding the behavior of charged particles in different physical systems, including space weather, fusion research, and astrophysical phenomena. They are often studied through theoretical modeling, laboratory experiments, and observations from spacecraft and telescopes.

In most cases, the Hall term has been ignored in applying Ohm's law as it has no marked effects for small and moderate values of the magnetic field. However, the current trend in the application of magnetohydrodynamics is toward a strong magnetic field so that the influence of electromagnetic force is noticeable. Under these conditions, the Hall current is important and has marked effects on the magnitude and direction of the current density and, consequently, on the magnetic force term. Therefore, it is necessary to study the effect of the Hall current on the flow. Interest in copper nanoparticles arises from the useful properties of this metal such as the good thermal and electrical conductivities at a much lower cost than silver; this leads to potential application in cooling fluids for electronic systems and conductive inks.

Copper–water nanofluids are a type of nanofluid composed of water-dispersed copper nanoparticles. These nanofluids have attracted much interest because of their special qualities and possible uses in a wide range of fields. The potential benefits of copper–water nanofluids include increased thermal conductivity and heat transfer efficiency, as well as breakthroughs in different industrial processes, electronics cooling, and energy efficiency programs. Future advancements and uses in this subject are possible with continued study and development.

Akbar *et al.*[23] studied the effects of entropy and induced magnetic field on the peristaltic flow of copper–water nanofluid. It had been observed that the entropy generation number and temperature increase with the increase in the Brinkman number.

By Abbasi *et al.*,[24] peristaltic transport of copper–water nanofluid saturating porous media had been developed. The findings showed that when the volume fraction of nanoparticles increases, the axial velocity of the copper–water nanofluid decreases. Copper nanoparticles also demonstrate an increase in the heat transfer between the fluid and solid boundary, making them an effective coolant. In addition, the fluid's temperature drops as the porous medium's permeability increases.

In the presence of a constant magnetic field, the Ohmic heating, and the Hall effects, Abbasi *et al.*[25] investigated the peristaltic transport of a silver–water nanofluid.

Based on the results, the base fluid (in this example, water) has a 16% lower temperature and nearly a 10% lower velocity when 5% silver nanoparticles are added. The variations in the state of the nanofluid caused by an applied magnetic field are lessened when Hall effects are present. The maximum temperature increases as the thermal slip parameter increases, whereas the maximum velocity of the nanofluid drops as the velocity slip parameter increases. The heat transfer inside horizontal and vertical enclosures filled with Cu–water nanofluid is studied by Hassan.[26] The results show that the average Nusselt number on the heat source increases with an increase in the Rayleigh number and volume fraction of Cu nanoparticles and with the decreasing diameter of Cu nanoparticles. At low Ra number (Ra = 10^3), the average Nusselt number increases with the increasing number of fins and increasing L/H. At a high Raleigh number (Ra = 10^6), an increase in the value of L/H has no great effect on the average Nusselt number. At a high Rayleigh number (Ra = 10^6), low nanoparticle diameter, and high volume fraction, the enclosure with a heat sink of one fin and L/H of 0.5 has the maximum average Nusselt number for horizontal and vertical enclosure. Iftikhar *et al.*[27] addressed the influence of wall properties on the peristaltic flow of Cu–water nanofluid in a non-uniform inclined tube. Thermal and velocity slip effects are taken into account. The results revealed that the temperature and velocity decrease by increasing values of nanoparticle volume fraction. Furthermore, velocity increases for increasing values of rigidity parameter, stiffness parameter, and viscous damping force parameter. In the presence of mixed convection and velocity and thermal slip conditions, peristaltic transport of copper–water nanofluid in an inclined channel is reported by Abbasi *et al.*[28] According to the obtained results, the temperature, trapping, axial velocity at the channel center, and pressure gradient are all decreased when copper nanoparticles are added. Increasing the velocity slip parameter reduces the velocity near the channel center. It also turned out that the presence of copper nanoparticles significantly boosts the heat transfer rate at the wall. Das *et al.*[29] investigated the combined effects of Hall and ion-slip currents on the peristaltic transport of a water-based nanofluid in an asymmetric channel in the presence of a high magnetic field. The results indicated that the presence of Hall and ion-slip currents causes the temperature function to exhibit a declining tendency. In addition, the axial pressure gradient is lessened by the incorporation of Hall and ion-slip currents. In the presence of the dominant magnetic field and Hall and ion-slip currents, Das *et al.*[30] perform an analytical simulation for the electro-osmosis modulated peristaltic transport of ionic hybrid nano-liquid with Casson model through a symmetric vertical microchannel occupying a homogeneous porous material. The results indicate that the ionic liquid's velocity is significantly influenced by Hall, ion-slip, and electroosmotic factors. Higher thermal Grashof number, electro-osmotic parameter, and Hall and ion-slip parameters all indicate an enhanced pressure gradient. However, it is decreased as a result of increased Hartmann number estimations.

Rafiq *et al.*[31] addressed the peristaltic flow of viscous nanofluid in a channel with compliant walls in the presence of Hall and ion-slip effects. According to the findings, the temperature and concentration of nanoparticles both effectively increase as the strength of Brownian motion effects increases. Comparable outcomes are noted for the ion-slip and Hall parameters. Furthermore, Hall and ion-slip parameters have an increasing influence on the heat transfer coefficient. In addition, a reduction in the trapped bolus's size is demonstrated for the ion-slip and Hall parameters. The combined effects of heat transfer and Hall and ion-slip currents in the peristaltic flow of nanofluids have implications in various technological domains. These include microfluidics, biomedical engineering (such as drug-delivery systems or biomedical diagnostics), renewable energy technologies (such as MHD generators or solar thermal systems), and advanced materials processing (such as nanofluid-based cooling of machining processes).

With regard to the foregoing explanation, this study aims to investigate the effects of heat transfer and Hall and ion-slip currents on the peristaltic flow of copper–water nanofluid. The structure of this essay is as follows: Sec. II contains the formulation of the problem. In Sec. III, the rate of volume flow. Section IV presents the solution to the problem under consideration. Section V deals with the results, discussion, and trapping phenomenon. The conclusions have been summarized in Sec. VI.

II. FORMULATION OF THE PROBLEM

Consider the peristaltic flow in a two-dimensional infinite horizontal asymmetric channel with a width of $d_1 + d_2$ filled with an incompressible viscous electrically conducting copper–water nanofluid. By supposing that the peristaltic wave trains traveling down the walls at constant speed c_1 have various amplitudes and phases, asymmetry in the channel is created (according to Fig. 1). Here, the Cartesian coordinates system is set up so that the X axis runs the whole length of the channel and the Y axis is perpendicular to it. The channel walls' forms are displayed as

$$H_1(X,t) = d_1 + a_1 \cos\left(\frac{2\pi}{\lambda}[X - c_1 t]\right), \quad \text{top wall}, \tag{1}$$

$$H_2(X,t) = -d_2 - a_2 \cos\left(\frac{2\pi}{\lambda}[X - c_1 t] + \omega\right), \quad \text{bottom wall}, \tag{2}$$

where a_1 and a_2 are the amplitudes of the upper and lower waves, respectively; λ is the wave length; c_1 is the propagation velocity; t is the time; X is the direction in which the wave is propagating; and ω is the phase difference in the range of $0 \le \omega \le \pi$. Note that $\omega = 0$ denotes an asymmetric channel with out-of-phase waves, whereas $\omega = \pi$ denotes a channel with in-phase waves. In addition, the variables d_1, d_2, a_1, a_2, and ω fulfill the following inequality:

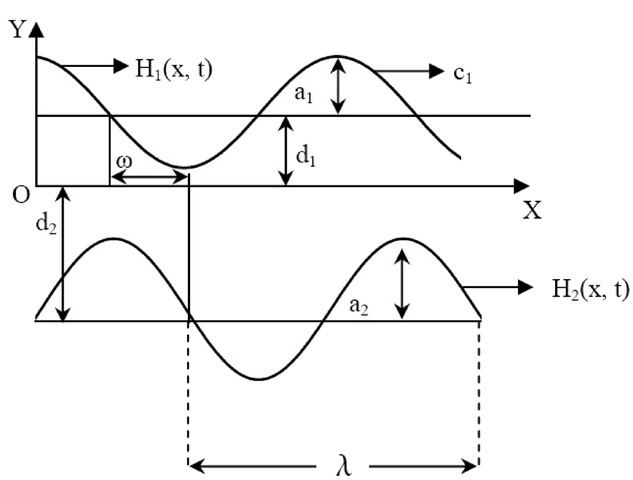

FIG. 1. Geometry of the problem.

$$a_1^2 + a_2^2 + 2a_1 a_2 \cos\omega \le (d_1 + d_2)^2, \tag{3}$$

to prevent the walls from interacting.

By applying a uniform magnetic field with a magnetic flux density $\mathbf{B} = (0, 0, B_0)$ and using an extremely small magnetic Reynolds number, the induced magnetic field can be ignored. In the absence of an externally applied electric field, we assume that the electric field vector equals zero. It is possible to express the current density J, which includes Hall and ion-slip currents, using the following formula:

$$\mathbf{J} = \frac{\sigma_{\text{eff}}\alpha_e}{\alpha_e^2 + \beta_e^2}(\mathbf{E} + \mathbf{V}\times\mathbf{B}) - \frac{\sigma_{\text{eff}}\beta_e}{\alpha_e^2 + \beta_e^2}(\mathbf{E} + \mathbf{V}\times\mathbf{B}) \times \frac{\mathbf{B}}{B_0}, \tag{4}$$

where $\mathbf{J}$ is the current density, σ_{eff} is the effective electric conductivity of copper–water nanofluid, $\mathbf{E}$ is the intensity of the electric field, $\mathbf{V} = [\bar{U}(\bar{X},\bar{Y},t), \bar{V}(\bar{X},\bar{Y},t), 0]$ is the velocity field, $\mathbf{B}$ is the magnetic field, and $\alpha_e = 1 + \beta_i\beta_e$, where β_i is the ion-slip parameter and β_e is the Hall parameter.

The heat transfer and nanoparticle processes are maintained by considering temperatures T_0 and $T_1(> T_0)$ and nanoparticle phenomena C_0 and $C_1(> C_0)$ to the upper and lower sides of the channel, respectively. Here, the fluid is a water-based nanofluid containing copper. The nanofluid is a two-component mixture with the following assumptions: incompressible; no chemical reactions; negligible viscous dissipation; negligible radiative heat transfer; and nano-solid particles and the base fluid are in thermal equilibrium.

The equations governing the two-dimensional motion of this model are as follows:

$$\frac{\partial \bar{U}}{\partial \bar{X}} + \frac{\partial \bar{V}}{\partial \bar{Y}} = 0, \tag{5}$$

$$\begin{aligned}\rho_{\text{eff}}\left(\frac{\partial \bar{U}}{\partial t} + \bar{U}\frac{\partial \bar{U}}{\partial \bar{X}} + \bar{V}\frac{\partial \bar{U}}{\partial \bar{Y}}\right) = &-\frac{\partial \bar{P}}{\partial \bar{X}} + \mu_{\text{eff}}\left(\frac{\partial^2 \bar{U}}{\partial \bar{X}^2} + \frac{\partial^2 \bar{U}}{\partial \bar{Y}^2}\right)\\ &- \frac{\sigma_{\text{eff}}B_0^2}{\alpha_e^2 + \beta_e^2}(\alpha_e\bar{U} - \beta_e\bar{V})\\ &+ g(\rho\beta)_{\text{eff}}(T - T_0)\\ &+ g(\rho\beta)_{\text{eff}}(C - C_0),\end{aligned} \tag{6}$$

$$\begin{aligned}\rho_{\text{eff}}\left(\frac{\partial \bar{V}}{\partial t} + \bar{U}\frac{\partial \bar{V}}{\partial \bar{X}} + \bar{V}\frac{\partial \bar{V}}{\partial \bar{Y}}\right) = &-\frac{\partial \bar{P}}{\partial \bar{Y}} + \mu_{\text{eff}}\left(\frac{\partial^2 \bar{V}}{\partial \bar{X}^2} + \frac{\partial^2 \bar{V}}{\partial \bar{Y}^2}\right)\\ &- \frac{\sigma_{\text{eff}}B_0^2}{\alpha_e^2 + \beta_e^2}(\alpha_e\bar{V} + \beta_e\bar{U}),\end{aligned} \tag{7}$$

$$\begin{aligned}&(\rho c)_{\text{eff}}\left(\frac{\partial T}{\partial t} + \bar{U}\frac{\partial T}{\partial \bar{X}} + \bar{V}\frac{\partial T}{\partial \bar{Y}}\right)\\ &\quad = k_{\text{eff}}\left(\frac{\partial^2 T}{\partial \bar{X}^2} + \frac{\partial^2 T}{\partial \bar{Y}^2}\right) + (\rho c)_p\Bigg[D_B\left(\frac{\partial C}{\partial \bar{X}}\frac{\partial T}{\partial \bar{X}} + \frac{\partial C}{\partial \bar{Y}}\frac{\partial T}{\partial \bar{Y}}\right)\\ &\qquad + \frac{D_T}{T_0}\left(\left(\frac{\partial T}{\partial \bar{X}}\right)^2 + \left(\frac{\partial T}{\partial \bar{Y}}\right)^2\right)\Bigg],\end{aligned} \tag{8}$$

$$\frac{\partial C}{\partial t} + \bar{U}\frac{\partial C}{\partial \bar{X}} + \bar{V}\frac{\partial C}{\partial \bar{Y}} = D_B\left(\frac{\partial^2 C}{\partial \bar{X}^2} + \frac{\partial^2 C}{\partial \bar{Y}^2}\right) + \frac{D_T}{T_0}\left(\frac{\partial^2 T}{\partial \bar{X}^2} + \frac{\partial^2 T}{\partial \bar{Y}^2}\right). \tag{9}$$

TABLE I. Numerical values of thermo-physical properties of water and copper.

Physical properties	Water (H_2O)	Copper (Cu)
ρ (kg/m^3)	997.1	8933
C (J/kg K)	4179	385
$\beta \times 10^5$ (K^{-1})	210	16.65
K (W/mK)	0.613	401
σ (S/m)	0.05	5.96×10^7

In the above equations, $\bar{P}(\bar{X}, \bar{Y}, t)$ is the pressure, g is the gravitational acceleration, D_B is the Brownian diffusion factor, and D_T is the coefficient of thermophoretic diffusion. For a two-phase flow model, the effective density ρ_{eff}, effective specific heat $(\rho c)_{\text{eff}}$, effective viscosity μ_{eff}, effective thermal conductivity k_{eff}, effective thermal expansion $(\rho\beta)_{\text{eff}}$, and effective electric conductivity σ_{eff} are taken in the following form:[23,24]

$$\rho_{\text{eff}} = (1-\phi)\rho_f + \phi\rho_p, \quad (\rho c)_{\text{eff}} = (1-\phi)(\rho c)_f + \phi(\rho c)_p,$$
$$\mu_{\text{eff}} = \frac{\mu_f}{(1-\phi)^{2.5}},$$

$$(\rho\beta)_{\text{eff}} = (1-\phi)(\rho\beta)_f + \phi(\rho\beta)_p, \quad \frac{k_{\text{eff}}}{k_f} = \frac{k_p + 2k_f - 2\phi(k_f - k_p)}{k_p + 2k_f + \phi(k_f - k_p)},$$

$$\frac{\sigma_{\text{eff}}}{\sigma_f} = 1 + \frac{3\left(\frac{\sigma_p}{\sigma_f} - 1\right)\phi}{\left(\frac{\sigma_p}{\sigma_f} + 2\right) - \left(\frac{\sigma_p}{\sigma_f} - 1\right)\phi}, \tag{10}$$

in which ϕ is the volume fraction of nanoparticles and the subscripts f and p, respectively, stand for the fluid and nanoparticles phase. The thermo-physical properties of pure water and copper at room temperature used in this study are presented in Table I.

The problem presented by the equations above is unsteady. Therefore, to make it steady, we convert it into a frame of reference traveling at the same speed along the wave. The conversion of the wave frame of reference $(\bar{x}, \bar{y})$ from the laboratory frame of reference $(\bar{X}, \bar{Y})$ is defined as

$$\bar{x} = \bar{X} - c_1\bar{t}, \quad \bar{y} = \bar{Y}, \quad \bar{u} = \bar{U} - c_1, \quad \bar{v} = \bar{V}, \quad \text{and} \quad \bar{p}(\bar{x}) = \bar{P}(\bar{x}, \bar{t}), \tag{11}$$

where the pressure and velocity components, respectively, in the wave and fixed frames of reference, are denoted by $(\bar{u}, \bar{v})$, $\bar{p}$ and $(\bar{U}, \bar{V})$, $\bar{P}$. By constructing the following quantities to represent the fluid flow in a non-dimensional form:

$$x = \frac{\bar{x}}{\lambda}, \quad y = \frac{\bar{y}}{d_1}, \quad u = \frac{\bar{u}}{c_1}, \quad v = \frac{\bar{v}}{c_1\lambda}, \quad h_1 = \frac{\bar{H}_1}{d_1},$$
$$h_2 = \frac{\bar{H}_2}{d_1}, \quad \delta = \frac{d_1}{\lambda}, \quad a = \frac{a_1}{d_1}, \quad b = \frac{a_2}{d_1},$$

$$d = \frac{d_2}{d_1}, \quad t = \frac{c_1\bar{t}}{\lambda}, \quad p = \frac{\bar{p}d_1^2}{c_1\lambda\mu_f}, \quad R_e = \frac{\rho_f d_1 c_1}{\mu_f},$$
$$M = \sqrt{\frac{\sigma_f}{\mu_f}}B_0 d_1, \quad \theta = \frac{T - T_0}{T_1 - T_0},$$

$$\Omega = \frac{C - C_0}{C_1 - C_0}, \quad N_b = \frac{(\rho c)_p D_B(C_1 - C_0)}{k_f}, \quad N_t = \frac{(\rho c)_p D_T(T_1 - T_0)}{k_f T_0},$$
$$Gr = \frac{\rho_f\beta_f g(T_1 - T_0)d_1^2}{\mu_f c_1}, \quad Br = \frac{\rho_f\beta_f g(C_1 - C_0)d_1^2}{\mu_f c_1}, \tag{12}$$

where δ is the dimensionless wave number, R_e is the Reynolds number, M is the Hartmann number, N_b is the Brownian motion parameter, N_t is the thermophoresis parameter, Gr is the local temperature Grashof number, and Br is the local nanoparticle Grashof number.

Using a long wave length approximation implies that the half channel width is less than the wave length of peristaltic wave, and a low Reynolds number approximation indicates an inertia free flow $(R_e \approx 0)$[29] together with the transformation in Eq. (11) and the previously stated non-dimensional parameters in Eq. (12); the governing equations in dimensionless form for this model will look like the following (with $u = \frac{\partial\psi}{\partial y}$, $v = -\frac{\partial\psi}{\partial x}$):

$$\frac{\partial p}{\partial x} = \frac{1}{(1-\phi)^{2.5}}\frac{\partial^3\psi}{\partial y^3} - A_1 M^2\frac{\alpha_e}{(\alpha_e^2 + \beta_e^2)}\left(\frac{\partial\psi}{\partial y} + 1\right)$$
$$+ A_2(Gr\theta + Br\Omega), \tag{13}$$

$$\frac{\partial p}{\partial y} = 0, \tag{14}$$

$$A_3\frac{\partial^2\theta}{\partial y^2} + N_b\frac{\partial\theta}{\partial y}\frac{\partial\Omega}{\partial y} + N_t\left(\frac{\partial\theta}{\partial y}\right)^2 = 0, \tag{15}$$

$$\frac{\partial^2\Omega}{\partial y^2} + \frac{N_t}{N_b}\frac{\partial^2\theta}{\partial y^2} = 0, \tag{16}$$

where

$$A_1 = 1 + \frac{3\left(\frac{\sigma_p}{\sigma_f} - 1\right)\phi}{\left(\frac{\sigma_p}{\sigma_f} + 2\right) - \left(\frac{\sigma_p}{\sigma_f} - 1\right)\phi}, \quad A_2 = 1 - \phi + \phi\frac{\rho_p\beta_p}{\rho_f\beta_f},$$
$$A_3 = \frac{k_p + 2k_f - 2\phi(k_f - k_p)}{k_p + 2k_f + \phi(k_f - k_p)}. \tag{17}$$

By eliminating the pressure between (13) and (14), we get

$$\frac{\partial^4\psi}{\partial y^4} - A_1 M^2\frac{\alpha_e}{\alpha_e^2 + \beta_e^2}(1-\phi)^{2.5}\frac{\partial\psi^2}{\partial y^2}$$
$$+ A_2(1-\phi)^{2.5}\left(Gr\frac{\partial\theta}{\partial y} + Br\frac{\partial\Omega}{\partial y}\right) = 0. \tag{18}$$

The relevant boundary conditions are

$$\psi = \frac{F}{2}, \quad \frac{\partial\psi}{\partial y} = -1, \quad \text{at} \quad y = h_1(x), \tag{19}$$

$$\psi = -\frac{F}{2}, \quad \frac{\partial\psi}{\partial y} = -1, \quad \text{at} \quad y = h_2(x), \tag{20}$$

$$\theta = 0, \quad \Omega = 0, \quad \text{at} \quad y = h_1(x), \tag{21}$$

$$\theta = 1, \quad \Omega = 1, \quad \text{at} \quad y = h_2(x), \tag{22}$$

where

$$h_1(x) = 1 + a\cos 2\pi x, \quad h_2(x) = -d - b\cos(2\pi x + \omega). \tag{23}$$

III. VOLUME FLOW RATE

The formula for the volume flow rate in the wave frame of reference is

$$q = \int_{h_2(x)}^{h_1(x)} u(x,y)dy, \tag{24}$$

where h_1 and h_2 are the functions of x alone.

The instantaneous volume flow rate in the fixed frame is represented by

$$Q = \int_{H_2(x,t)}^{H_1(x,t)} [u(x,y,t) + c]dy = q + ch_1 - ch_2, \tag{25}$$

in which H_1 and H_2 are the functions of x and t.

The time-mean flow over time period $T = \lambda/c$ at a fixed position is given by

$$\begin{aligned}\bar{Q}(x,t) &= \frac{1}{T}\int_0^T Q(x,y)dt\\ &= \frac{1}{T}\int_0^T (q + ch_1 - ch_2)dt\\ &= q + cd_1 + cd_2.\end{aligned} \tag{26}$$

If we find the dimensionless mean flow Θ in the laboratory frame and F in the wave frame according to

$$\Theta = \frac{\bar{Q}}{cd_1}, \quad F = \frac{q}{cd_1}, \tag{27}$$

one finds that Eq. (27) becomes

$$\Theta = F + 1 + d, \tag{28}$$

where

$$F = \int_{h_2}^{h_1} u\, dy. \tag{29}$$

IV. SOLUTION OF THE PROBLEM

The exact solutions for stream function, temperature profile, nanoparticle concentration, and pressure gradient can be written as

$$\begin{aligned}\Psi = {} & C_5 + C_6 y + C_7\cosh\left(\frac{y\sqrt{\alpha_e^2 M^2 A_1(1-\phi)^{2.5}}}{(\alpha_e^2+\beta_e^2)}\right)\\ & + C_8\sinh\left(\frac{y\sqrt{\alpha_e^2 M^2 A_1(1-\phi)^{2.5}}}{(\alpha_e^2+\beta_e^2)}\right)\\ & - \frac{A_2A_3^3(1-\phi)^{2.5}C_4(x)(N_bGr - N_tBr)e^{\frac{-yC_1(x)N_b}{A_3}}}{C_1(x)N_b^2[C_1^2(x)N_b^2 - A_1A_3^2M^2(1-\phi)^{2.5}]}\\ & + \frac{A_2BrC_1(x)y^2}{2A_1M^2},\end{aligned}$$

$$\theta(x,y) = C_3(x) + C_4(x)e^{\frac{-N_bC_1(x)y}{A_3}}, \tag{31}$$

$$\Omega(x,y) = C_2(x) + C_1(x)y - \frac{N_t}{N_b}\left[C_3(x) + C_4(x)e^{\frac{-N_bC_1(x)y}{A_3}}\right]. \tag{32}$$

The pressure gradient can be written in the following form:

$$\begin{aligned}\frac{\partial p}{\partial x} = {} & \frac{S_1^3}{(1-\phi)^{2.5}}[C_7\sinh(yS_1) + C_8\cosh(yS_1)] + A_2(Gr\theta + Br\Omega)\\ & - \frac{A_1M^2\alpha_e}{(\alpha_e^2+\beta_e^2)}\big[C_6 + S_1(C_7\sinh(yS_1) + C_8\cosh(yS_1))\\ & - S_2S_3e^{yS_3} + 2S_4y + 1\big],\end{aligned} \tag{33}$$

where

$$\begin{aligned} S_1 &= \frac{\sqrt{\alpha_e^2M^2A_1(1-\phi)^{2.5}}}{(\alpha_e^2+\beta_e^2)},\\ S_2 &= \frac{A_2A_3^3(1-\phi)^{2.5}C_4(x)(N_bGr - N_tBr)}{C_1(x)N_b^2[C_1^2(x)N_b^2 - A_1A_3^2M^2(1-\phi)^{2.5}]},\\ S_3 &= \frac{-N_bC_1(x)}{A_3}, \quad S_4 = \frac{A_2BrC_1(x)}{2A_1M^2},\end{aligned} \tag{34}$$

and $C_i(x)$, $i = 1,2,3,4$, are unknown functions to be determined. By applying the boundary conditions (21) and (22) on (31) and (32), and then solving the resulting equations, we get

$$C_1(x) = \frac{N_b + N_t}{N_b(h_2 - h_1)}, \quad C_2(x) = \frac{(N_b + N_t)h_1}{N_b(h_1 - h_2)}, \tag{35}$$

$$C_3(x) = \frac{e^{\frac{-N_bC_1(x)h_1}{A_3}}}{e^{\frac{-N_bC_1(x)h_1}{A_3}} - e^{\frac{-N_bC_1(x)h_2}{A_3}}}, \quad C_4(x) = \frac{1}{e^{\frac{-N_bC_1(x)h_2}{A_3}} - e^{\frac{-N_bC_1(x)h_1}{A_3}}}. \tag{36}$$

The constants C_i, $i = 5,6,7,8$, can be determined by applying the boundary conditions (19) and (20) on (30). (These constants can be easily obtained through using the Mathematica software.)

The non-dimensional pressure rise over one wave length for the axial velocity is given by

$$\Delta P_\lambda = \int_0^1 \left(\frac{\partial P}{\partial x}\right)dx. \tag{37}$$

The outcomes attained in this study exhibit strong agreement with those found in Refs. 11, 21, and 29. For example, the model represented by Asghar *et al.*[11] can be obtained if we put $\phi = 0$, $A_1 = 1$, $A_2 = 0$, and $Br = 0$. Furthermore, the model introduced by Akbar *et al.*[21] can be achieved by selecting $A_1 = 1$, $\alpha_e = 1$, $\beta_i = \beta_e = 0$, $A_2 = 1$, and $Br = 0$. We may now talk about the findings that we have discovered, which will be demonstrated in Sec. V.

V. THE FINDINGS AND DISCUSSION

In this section, we examine how various embedded factors affect the behavior of the pressure gradient, pressure rise, axial velocity, temperature, nanoparticle concentration, and streamlines at the wall.

The axial velocity is examined in Fig. 2 in relation to the Hartmann number M, nanoparticle volume fraction ϕ, Hall parameter β_e, and local temperature Grashof number Gr. It is evident from Fig. 2(a) that an increase in M produces a decrease in the magnitude of axial velocity at the channel center. This conclusion is consistent from a physical point of view with the well-known Hartmann result, which states that "increasing the magnetic field strength led to decay in the velocity." As the Hartmann number increases, the dominance of electromagnetic forces becomes more pronounced, leading to stronger effects on the fluid flow. This can result in velocity profiles where the fluid is pushed toward the channel walls due to electromagnetic forces, causing a decrease in the axial velocity at the center and an increase near the walls.

Figure 2(b) shows the influence of nanoparticle volume fraction on the axial velocity distribution. It is seen that the magnitude of velocity rises and reaches its greatest value close to the channel's center, while it decreases close to the channel's edges owing to an increase in ϕ. Increasing the volume fraction of nanoparticles in the nanofluid alters its rheological properties. Nanoparticles, such as copper particles in water, can affect the fluid's viscosity, thermal conductivity, and density. In general, adding nanoparticles increases the viscosity of the fluid, affecting its flow behavior.

According to Fig. 2(c), the magnitude of the velocity profile increased as the Hall parameter magnitude β_e increased. This is because by raising the magnetic field's intensity, the Hall effect becomes more resistant to any change in the fluid's condition. Increasing the Hall parameter can cause the fluid to be pushed toward the channel center due to the magnetic field's influence, resulting in higher axial velocities at the center and lower velocities near the channel walls. Figure 2(d) shows that, as Gr grows, the magnitude of velocity at the bottom side of the channel rises, which indicates that buoyancy forces resulting from the temperature gradient dominate viscous forces. At the channel's top walls, everything is the opposite. From the perspective of physics, this is because a higher Grashof number denotes a greater temperature differential between the channel's upper and bottom walls, which increases

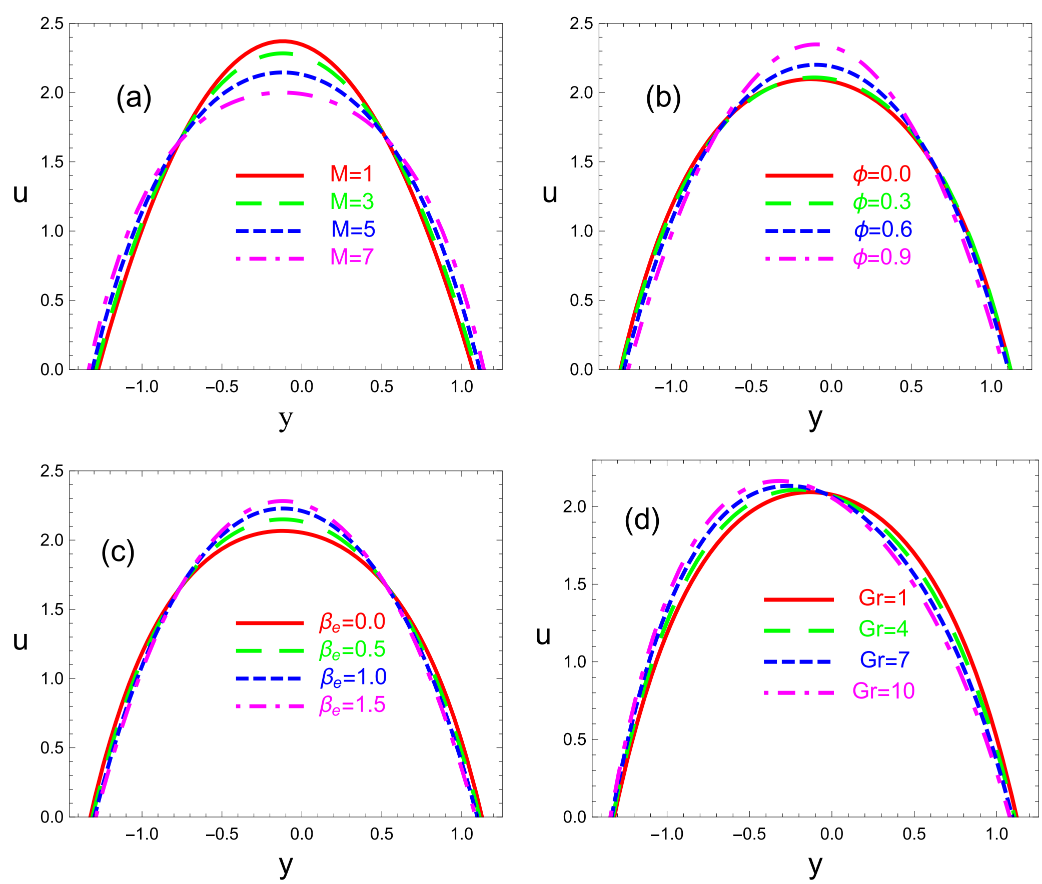

FIG. 2. (a)–(d) Variations of the velocity profile u with y for different values of the Hartmann number M, nanoparticle volume fraction ϕ, Hall parameter β_e, and local temperature Grashof number Gr, respectively. The additional factors selected are as follows: $F = 3.5, x = 1, d = 1, a = 0.3, b = 0.5, N_b = 0.8, N_t = 0.5, \phi = 0.1, Gr = 0.5, Br = 0.5, \omega = 0.2, \beta_i = 0.5, \beta_e = 1.5$ [panel (a)]; $F = 3.5, x = 1, d = 1, a = 0.3, b = 0.5, N_b = 0.8, N_t = 0.5, M = 2, Gr = 0.5, Br = 0.5, \omega = 0.2, \beta_i = 0.5, \beta_e = 1.5$ [panel (b)]; $F = 3.5, x = 1, d = 1, a = 0.3, b = 0.5, N_b = 0.8, N_t = 0.5, \phi = 0.1, Gr = 0.5, Br = 0.5, \omega = 0.2, \beta_i = 0.5, M = 2$ [panel (c)]; $F = 3.5, x = 1, d = 1, a = 0.3, b = 0.5, N_b = 0.8, N_t = 0.5, \phi = 0.1, M = 2, Br = 0.5, \omega = 0.2, \beta_i = 0.5, \beta_e = 1.5$ [panel (d)].

buoyant forces. This causes the fluid near the colder top wall to decelerate downhill and the fluid near the warmer bottom wall to accelerate upward.

Figure 3 shows the pressure gradient for various values of the Hartmann number M, nanoparticle volume fraction ϕ, Hall parameter β_e, and channel width d. It has been discovered that as M and ϕ grow, the magnitude of the pressure gradient increases; however, as β_e and d increase, the magnitude of the gradient reduces. In addition, it was noted that the pressure gradient is minimal close to the channel walls and reaches its highest value at the channel's center. As a result, the channel's midsection can now readily accommodate flow. The pressure gradient rises as M increases, as shown in Fig. 3(a). This may be understood physically as follows: In magnetohydrodynamic (MHD) flow, the Hartmann number indicates how important electromagnetic forces are in comparison to viscous forces. A higher Hartmann number indicates a stronger influence of the magnetic field on the flow. Consequently, increasing the Hartmann number can lead to more pronounced magnetic effects, such as magnetic damping or suppression of flow instabilities. In peristaltic flow, this can manifest as increased resistance to flow motion, necessitating higher pressure gradients to maintain fluid transport through the channel.

As we can see from Fig. 3(b), the pressure gradient rises as the nanoparticle volume fraction ϕ rises. In actuality, adding nanoparticles to the base fluid increases its viscosity due to the interaction between the nanoparticles and the fluid molecules. A higher nanoparticle volume fraction results in a more viscous nanofluid. This increased viscosity offers more resistance to flow, requiring a higher pressure gradient to overcome. Figure 3(c) demonstrates that the pressure gradient decreases as the Hall parameter β_e increases. The reason behind this is that the Hall effect plays a role in magnetic damping in the magnetohydrodynamic (MHD) flow, which resists fluid motion. The damping effect is lessened and greater fluid movement is permitted against the magnetic field by raising the Hall parameter. This lowers the pressure gradient needed to overcome the magnetic field's resistance and, ultimately, lowers the pressure gradient overall. As d increases, the pressure gradient reduces, as shown in Fig. 3(d). To maintain a constant mass flow rate, the fluid

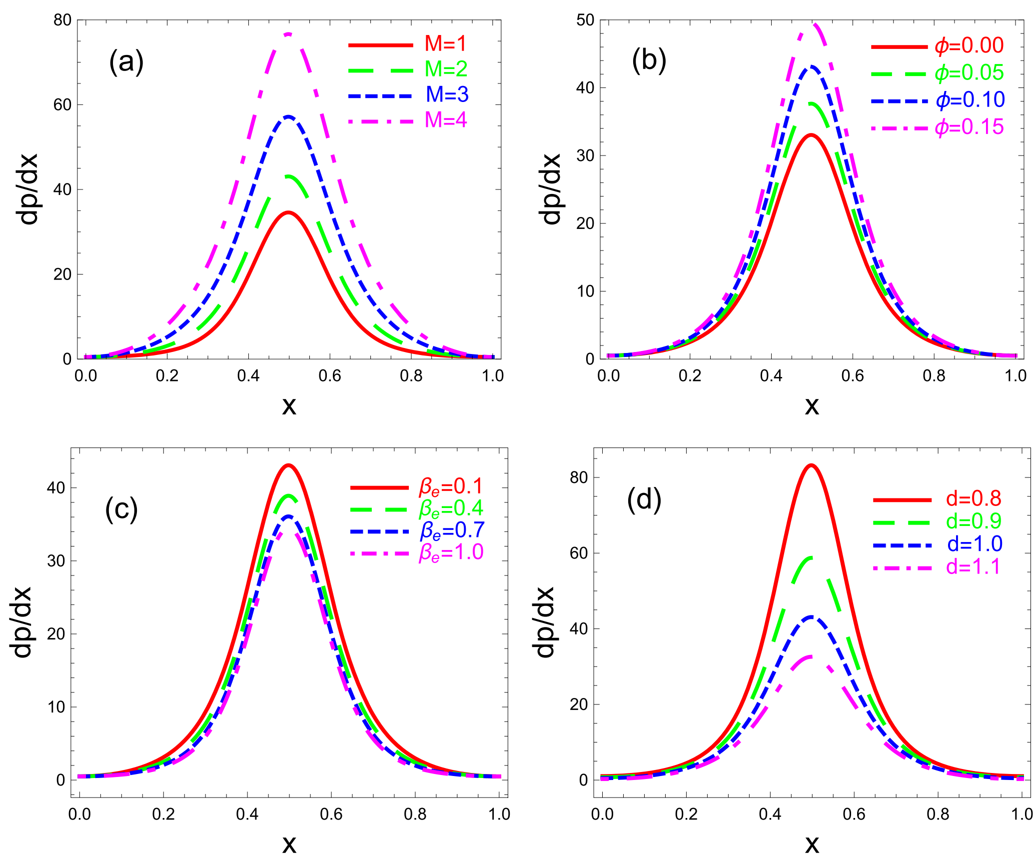

FIG. 3. (a)–(d) Variations of the axial pressure gradient $\frac{dp}{dx}$ with x for different Hartmann number M, nanoparticle volume fraction ϕ, Hall parameter β_e, and channel width d values, respectively. The other parameters chosen are as follows: $F = -3, d = 1, a = 0.3, b = 0.7, N_b = 0.8, N_t = 0.5, \phi = 0.1, \omega = 0.02, y = 1, Gr = 0.5, Br = 0.5, \beta_i = 0.5, \beta_e = 0.1$ [panel (a)]; $F = -3, d = 1, a = 0.3, b = 0.7, N_b = 0.8, N_t = 0.5, M = 2, \omega = 0.02, y = 1, Gr = 0.5, Br = 0.5, \beta_i = 0.5, \beta_e = 0.1$ [panel (b)]; $F = -3, d = 1, a = 0.3, b = 0.7, N_b = 0.8, N_t = 0.5, \phi = 0.1, \omega = 0.02, y = 1, Gr = 0.5, Br = 0.5, \beta_i = 0.5, M = 2$ [panel (c)]; $F = -3, M = 2, a = 0.3, b = 0.7, N_b = 0.8, N_t = 0.5, \phi = 0.1, \omega = 0.02, y = 1, Gr = 0.5, Br = 0.5, \beta_i = 0.5, \beta_e = 0.1$ [panel (d)].

velocity usually decreases as the channel width rises, in accordance with the principle of conservation of mass. The fluid's kinetic energy decreases in conjunction with this velocity drop, which lowers the pressure gradient.

In Fig. 4, it is examined how the local temperature Grashof number Gr, nanoparticle volume fraction ϕ, Hall parameter β_e, and ion-slip parameter β_i affect the dimensionless average rise in pressure ΔP_λ vs mean flow rate Θ. The expression of pressure rise as shown in Eq. (37) is computed numerically by using Mathematica software. This graph is divided into four regions as follows:

(i) The region $(\Theta > 0, \Delta P_\lambda > 0)$ refers to peristaltic pumping.
(ii) The region $(\Theta > 0, \Delta P_\lambda < 0)$ refers to augmented flow or co-pumping.
(iii) The region $(\Theta\langle 0, \Delta P_\lambda \rangle 0)$ refers to retrograde or backward pumping.
(iv) The region $(\Theta < 0, \Delta P_\lambda < 0)$ refers to that the flow is reversed to the focus of the peristaltic motion.

It is clear that there is a linear relation between the average rise in pressure and the mean flow rate. In addition, increasing Θ reduces the average rise in pressure. Furthermore, in the peristaltic region, the maximum mean flow rate is achieved at zero average rise in pressure and the maximum average rise in pressure is obtained at a zero mean flow rate. In Fig. 4(a), as the Grashof number increases, the pressure develops. This happens because increasing the Grashof number results in higher temperature gradients, which enhance buoyant forces. In a nanofluid, nanoparticles (such as copper nanoparticles) dispersed in the base fluid (water) can alter the thermophysical properties, potentially enhancing heat transfer. This increased buoyancy effect can lead to more vigorous fluid motion, resulting in higher pressure rises along the channel.

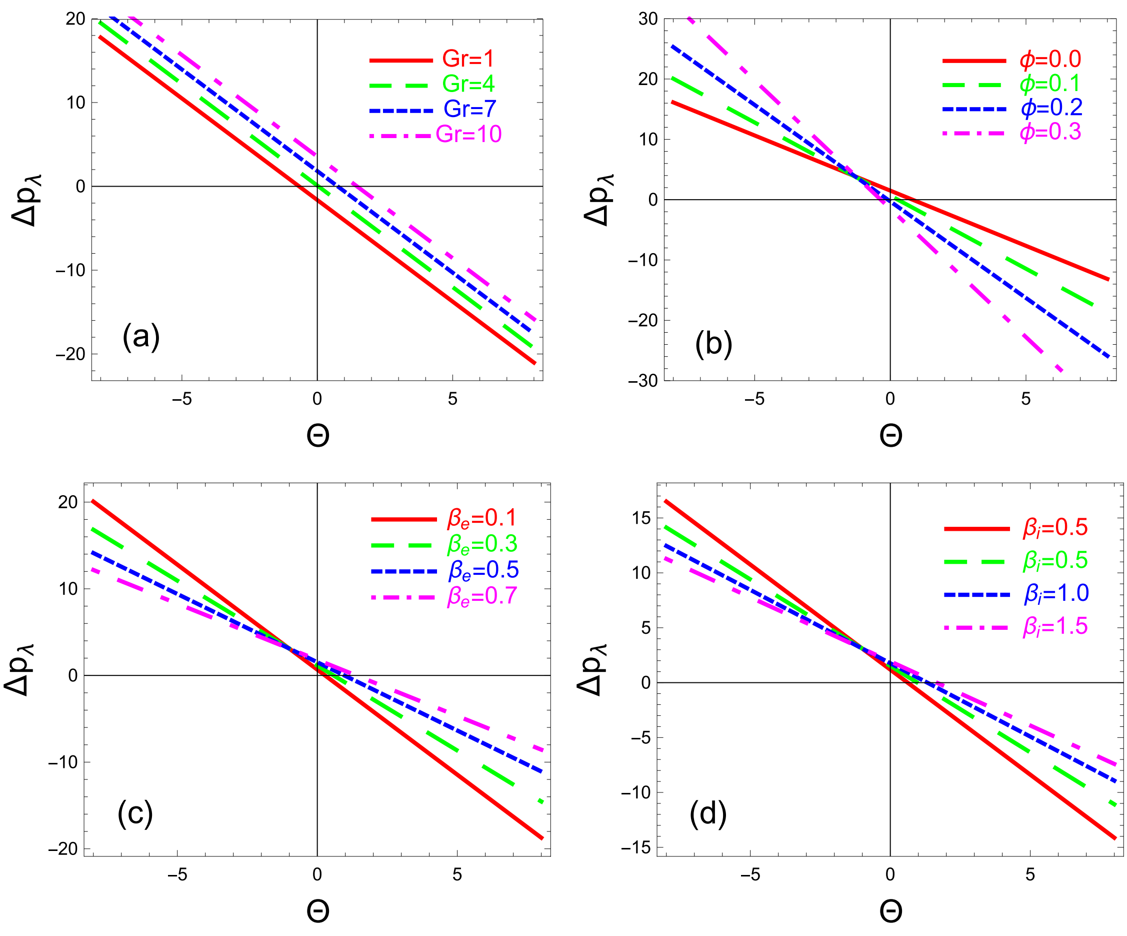

FIG. 4. (a)–(d) Variations of dimensionless average rise in pressure ΔP_λ against θ for various values of local temperature Grashof number Gr, nanoparticles volume fraction ϕ, Hall parameter β_e, ion-slip parameter β_i, respectively. The other parameters chosen are as follows: $N_b = 0.8, N_t = 0.5, d = 1, y = 1, a = 0.3, b = 0.7, M = 2, Br = 0.5, \phi = 0.1, \omega = 0.02, \beta_i = 0.5, \beta_e = 0.1$ [panel (a)]; $N_b = 0.8, N_t = 0.5, d = 1, y = 1, a = 0.3, b = 0.7, Gr = 5, Br = 0.5, M = 2, \omega = 0.02, \beta_i = 0.5, \beta_e = 0.1$ [panel b)]; $N_b = 0.8, N_t = 0.5, d = 1, y = 1, a = 0.3, b = 0.7, Gr = 5, Br = 0.5, \phi = 0.1, \omega = 0.02, \beta_i = 0.5, M = 2$ [panel (c)]; $N_b = 0.8, N_t = 0.5, d = 1, y = 1, a = 0.3, b = 0.7, Gr = 5, Br = 0.5, \phi = 0.1, \omega = 0.02, M = 2, \beta_e = 0.1$ [panel (d)].

Figure 4(b) depicts that increasing the nanoparticles volume fraction ϕ increases the pressure rise in the backward pumping region and decreases it in the co-pumping region. Physically speaking, this occurs because the thermophysical characteristics of the nanofluid, such as its viscosity and heat conductivity, change when the volume fraction of nanoparticles in the fluid increases. The net pressure rise in each zone is determined by the combined effects of higher viscosity and greater thermal conductivity resulting from the volume fraction of nanoparticles. In the backward-pumping zone, the dominant influence of increased viscosity outweighs the benefits of enhanced heat transfer, resulting in higher pressure rise. In contrast, in the co-pumping zone, the improved heat transfer dominates, leading to a reduction in pressure rise despite the increased viscosity. In Figs. 4(c) and 4(d), the situation is entirely inverted; as a result of raising Hall and ion-slip parameters, respectively, the pressure rise reduces in the backward pumping region and increases in the co-pumping region. It is known that the Hall parameter represents the relative strength of electromagnetic forces to fluid inertia, while the ion-slip parameter reflects the influence of ion mobility on the flow. Increasing Hall and ion-slip parameters in the peristaltic flow modifies the electromagnetic forces acting on the flow, resulting in decreased pressure rise in the backward-pumping zone and increased pressure rise in the co-pumping zone as follows: Increasing Hall and ion-slip parameters can weaken the oppositional effect of backward pumping by exerting electromagnetic forces that partially counteract the pressure gradient. As a result, the pressure rise in the backward-pumping zone decreases because the electromagnetic forces assist in overcoming the pressure gradient opposing the flow. Conversely, increasing Hall and ion-slip parameters can strengthen the aiding effect of co-pumping by enhancing the electromagnetic forces that align with the pressure gradient. This reinforcement of electromagnetic forces helps to drive the flow in the direction of the pressure gradient, resulting in increased pressure rise in the co-pumping zone.

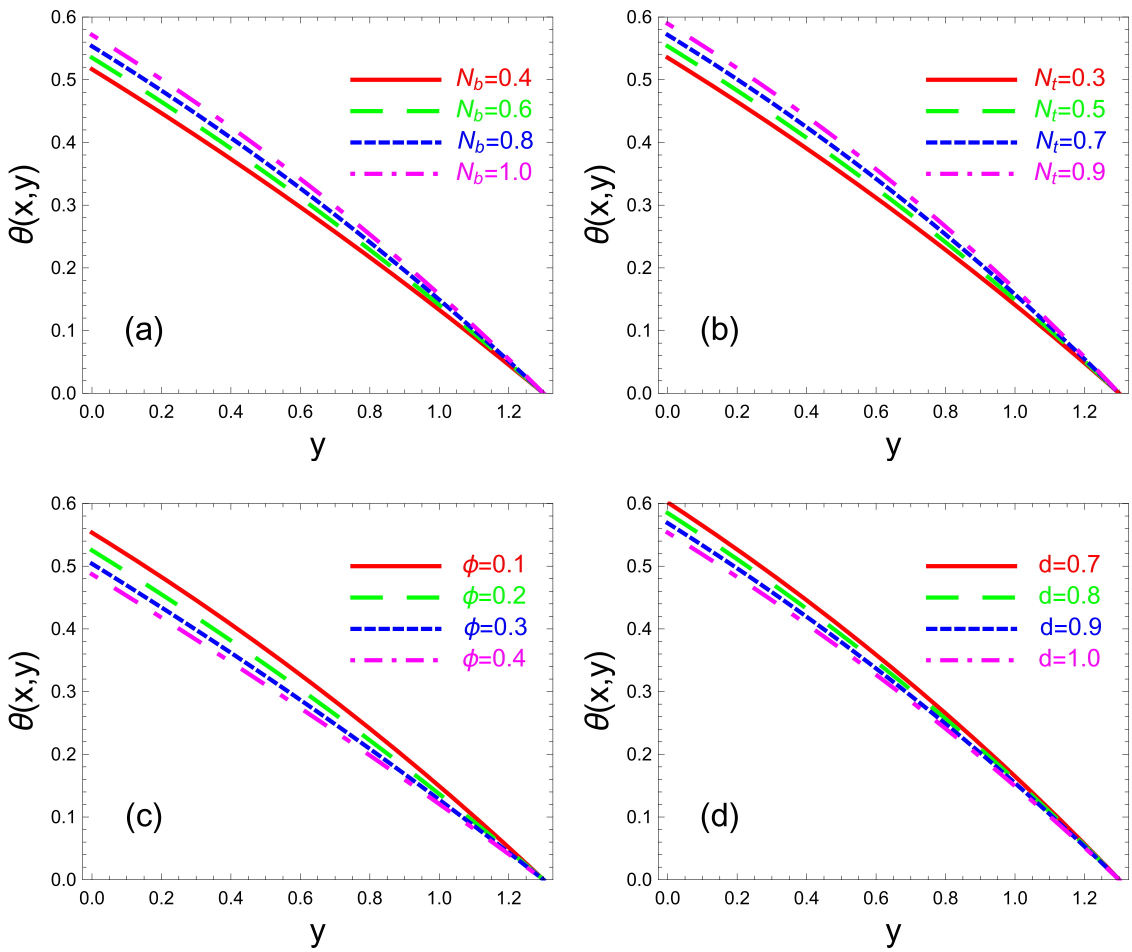

FIG. 5. (a)–(d) Different values of the Brownian motion parameter N_b, the thermophoresis parameter N_t, the nanoparticle volume fraction ϕ, the width of the channel d, and the fluid's local temperature $\theta(x, y)$ vs the space variable y, respectively. The other parameters chosen are as follows: $N_t = 0.5, x = 1, d = 1, a = 0.3, b = 0.7, \omega = 0.02, \phi = 0.1$ [panel (a)]; $N_b = 0.8, x = 1, d = 1, a = 0.3, b = 0.7, \omega = 0.02, \phi = 0.1$ [panel (b)]; $N_t = 0.5, x = 1, d = 1, a = 0.3, b = 0.7, \omega = 0.02, N_b = 0.8$ [panel (c)]; $N_t = 0.5, x = 1, N_b = 0.8, a = 0.3, b = 0.7, \omega = 0.02, \phi = 0.1$ [panel (d)].

The effects of the Brownian motion parameter N_b, the thermophoresis parameter N_t, the nanoparticle volume fraction ϕ, and the channel width d on the fluid's local temperature are studied in Fig. 5. It is obvious that as N_b and N_t are raised, the fluid's local temperature rises, as shown in Figs. 5(a) and 5(b). The random movement of nanoparticles dispersed in a fluid is referred to as Brownian motion, while the term "thermophoresis" describes how a temperature difference causes particles to migrate. Both Brownian motion and thermophoresis can contribute to enhancing the thermal conductivity of the nanofluid. The increased movement of nanoparticles and their redistribution due to thermophoresis can lead to a more efficient transfer of heat within the fluid. Consequently, the nanofluid can exhibit higher thermal conductivity, which further promotes an increase in the local temperature. This is in accordance with the conclusion that a simultaneous increase in the Brownian motion and thermophoresis parameters produces an increase in the temperature especially for sufficiently stronger thermophoresis effects.

In Figs. 5(c) and 5(d), the situation is the opposite. The temperature of the base fluid is shown to be decreased with the addition of copper nanoparticles and an increase in the nanoparticle volume fraction. This is mainly due to the high thermal conductivity of copper nanoparticles, which leads to quicker heat transmission from the fluid to the ambient and prevents the fluid from attaining high temperatures. This conclusion is the main reason behind the successful use of copper nanoparticles as coolants in various industrial appliances. On the other hand, widening the channel [see Fig. 5(d)] increases the surface area available for heat transfer between the nanofluid and the channel walls. This increased surface area facilitates the heat dissipation from the nanofluid to the surroundings, effectively lowering the local temperature of the nanofluid.

The graphs shown in Fig. 6 are the nanoparticle concentration profiles for various values of the Brownian motion parameter N_b, the thermophoresis parameter N_t, the nanoparticle volume fraction ϕ, and the channel width d. The concentration of nanoparticles increases as N_b increases in Fig. 6(a). This is because a higher

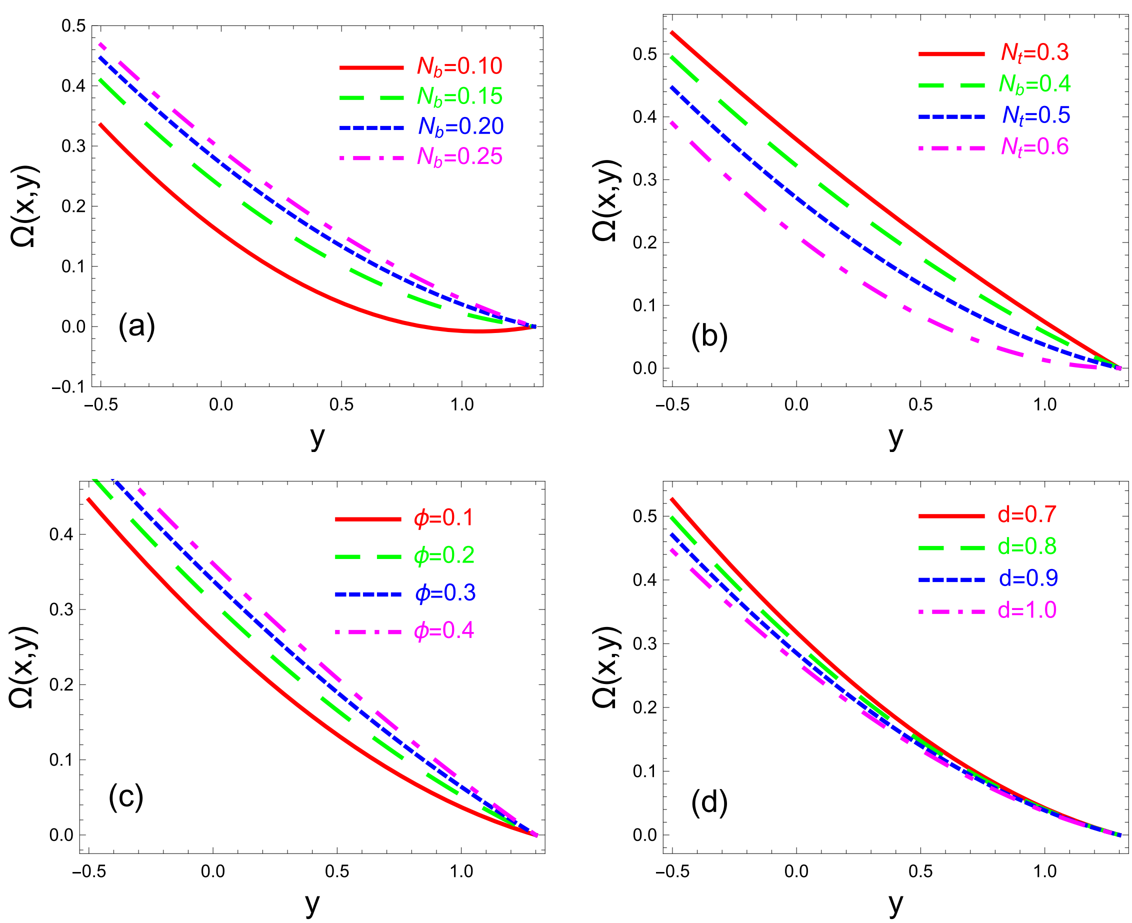

FIG. 6. (a)–(d) Nanoparticle concentration $\Omega(x, y)$ variations for various values of the Brownian motion parameter N_b, the thermophoresis parameter N_t, the nanoparticle volume fraction ϕ, and the channel width d, respectively. The other factors selected are as follows: $N_t = 0.5, x = 1, d = 1, a = 0.3, b = 0.7, \omega = 0.02, \phi = 0.1$ [panel (a)]; $N_b = 0.2, x = 1, d = 1, a = 0.3, b = 0.7, \omega = 0.02, \phi = 0.1$ [panel (b)]; $N_t = 0.5, x = 1, d = 1, a = 0.3, b = 0.7, \omega = 0.02, N_b = 0.2$ [panel (c)]; $N_t = 0.5, x = 1, N_b = 0.2, a = 0.3, b = 0.7, \omega = 0.02, \phi = 0.1$ [panel (d)].

Brownian motion value suggests a more vigorous kind of thermal agitation or random motion of the nanoparticles inside the nanofluid. The nanoparticles collide with the surrounding fluid molecules more often as a result. By distributing the nanoparticles more equally throughout the fluid, these collisions help stop them from settling or clumping together. As a result, improving the Brownian motion parameter encourages improved nanoparticle dispersion. As the thermophoresis parameter is increased, the concentration of nanoparticles falls, as shown in Fig. 6(b). This occurs as a result of increased nanoparticle migration into fluid areas with temperature gradients caused by raising the thermophoresis parameter, which may cause the nanofluid's total concentration of nanoparticles to drop. According to Fig. 6(c), the concentration of nanoparticles rises as the nanoparticle volume fraction parameter is raised. Naturally, as the nanoparticle volume fraction increases, more nanoparticles are dispersed throughout the fluid. This leads to better dispersion and less likelihood of nanoparticle aggregation or settling. Therefore, the nanofluid can accommodate a higher concentration of nanoparticles without phase separation or sedimentation. Figure 6(d) shows that when the channel width increases, the concentration of nanoparticles drops. In fact, as the channel width increases, the total volume of the channel also increases. If the same amount of nanofluid flows through the wider channel, it becomes more dispersed over a larger area. This effectively dilutes the nanofluid, resulting in a lower concentration of nanoparticles per unit volume.

A. Trapping phenomenon

The tendency of fluid particles to get trapped or have their mobility restricted inside specific areas of the flow field is known as the trapping phenomenon in the fluid flow. Numerous factors, including vortices, recirculation zones, boundary layer effects, or obstructions in the flow channel, can cause this confinement. Fluid dynamics is greatly affected by the trapping phenomenon, which can have an impact on heat transfer, mixing, and flow behavior as a whole. Understanding and characterizing the trapping phenomenon are crucial for various engineering and scientific applications, as they influence the performance and efficiency of fluid systems and devices.

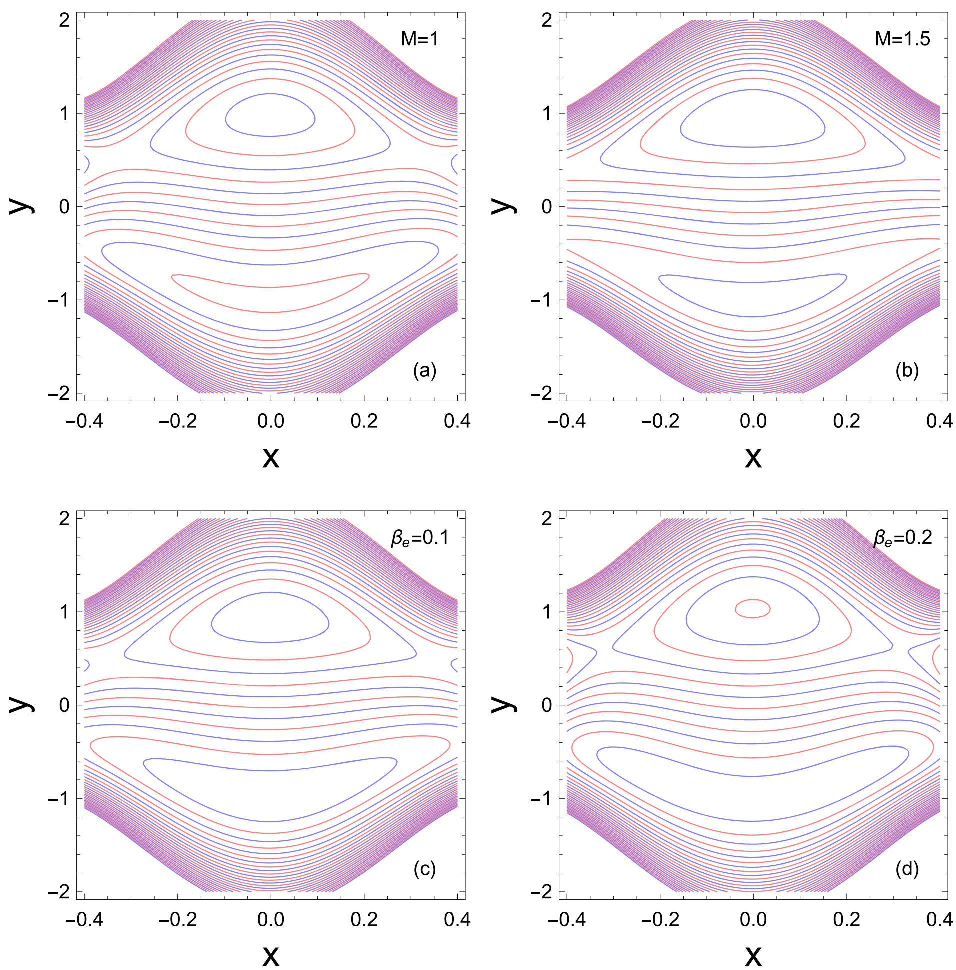

FIG. 7. Streamlines for different values of (a) and (b) Hartmann number M and (c) and (d) Hall parameter β_e. The other parameters chosen are as follows: $F = 0.2$, $d = 1$, $a = 0.5$, $b = 0.5$, $\phi = 0.2$, $N_b = 0.8$, $N_t = 0.5$, $Gr = 1$, $Br = 0.5$, $\omega = 0.02$, $\beta_i = 0.3\beta_e = 0.15$ [panels (a) and (b)]; $F = 0.2$, $d = 1$, $a = 0.5$, $b = 0.5$, $\phi = 0.2$, $N_b = 0.8$, $N_t = 0.5$, $Gr = 1$, $Br = 0.5$, $\omega = 0.02$, $\beta_i = 0.3$, $M = 1$ [panels (c) and (d)].

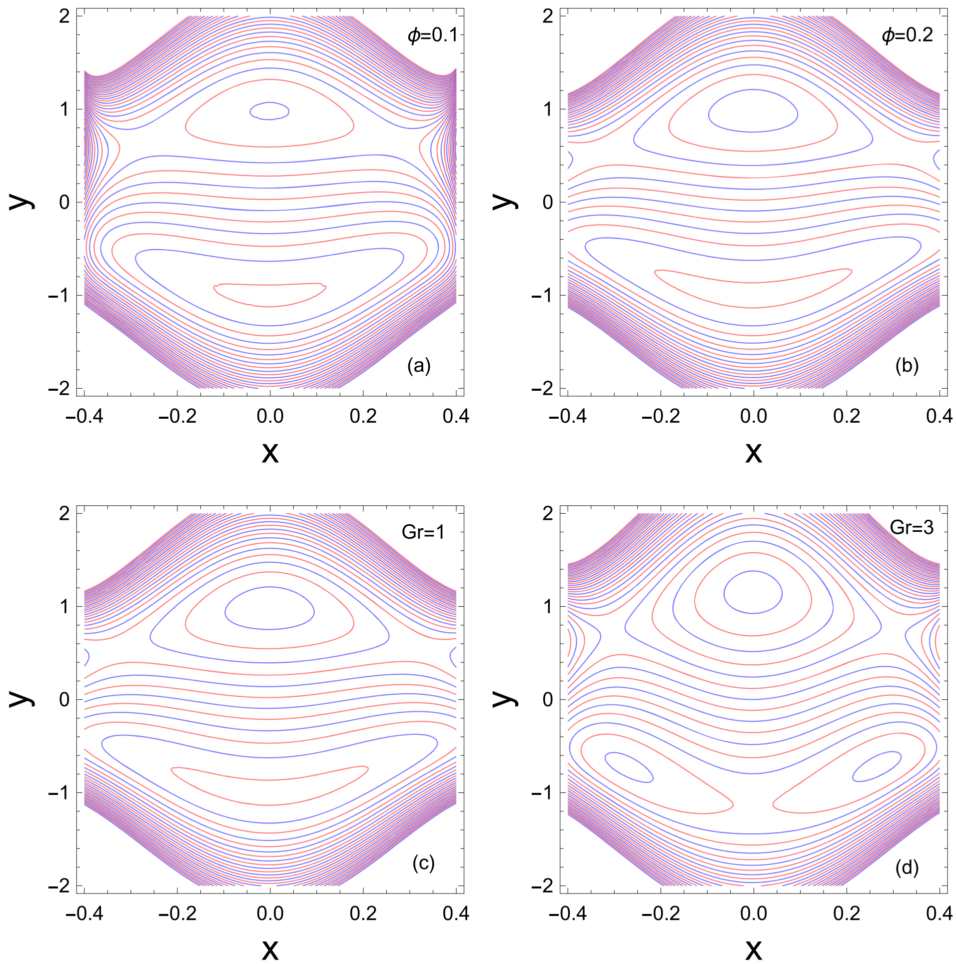

FIG. 8. Streamlines for different values of (a) and (b) nanoparticle volume fraction ϕ and (c) and (d) local temperature Grashof number Gr. The other parameters chosen are as follows: $F = 0.2$, $d = 1$, $a = 0.5$, $b = 0.5$, $M = 1$, $N_b = 0.8$, $N_t = 0.5$, $Gr = 1$, $Br = 0.5$, $\omega = 0.02$, $\beta_i = 0.3\beta_e = 0.15$ [panels (a) and (b)]; $F = 0.2$, $d = 1$, $a = 0.5$, $b = 0.5$, $\phi = 0.2$, $N_b = 0.8$, $N_t = 0.5$, $M = 1$, $Br = 0.5$, $\omega = 0.02$, $\beta_i = 0.3$, $M = 1$ [panels (c) and (d)].

Figures 7 and 8 depict the trapping for various values of the Hartmann number M, Hall parameter β_e, nanoparticle volume fraction ϕ, and the local temperature Grashof number Gr. Figures 7(a) and 7(b) show that when M grows, the size of the trapped bolus expands in the top section of the channel and contracts in the lower half. This can be explained physically as follows: When the Hartmann number increases, it implies a stronger magnetic field effect. A stronger magnetic field tends to exert greater force on the conducting fluid, causing it to resist movement perpendicular to the magnetic field lines. As a result, the boluses of fluid are more likely to be pushed upward against the magnetic field lines in the upper half of the channel.

This can lead to larger trapped boluses in this region. Conversely, in the lower half of the channel, the effect of the magnetic field combined with other currents (such as Hall and ion-slip currents) might counteract the peristaltic motion, causing the fluid to experience less trapping or pooling in this region. This results in smaller or fewer trapped boluses in the lower half of the channel.

In the same context, if we raised the magnitude of β_e, as shown in Figs. 7(c) and 7(d), the number of trapped boluses rises exclusively in the upper portion of the channel and its size grows in the bottom half of the channel. This could be because increasing the Hall parameter indicates a greater magnetic Hall effect, which modifies the fluid flow behavior. Because the magnetic field pushes the charged nanofluid particles in a direction perpendicular to the magnetic field lines and the flow direction, this action increases the number of trapped boluses in the top half. On the other hand, the magnetic Hall effect and peristaltic motion interact differently in the lower half of the channel. These two actions work together to promote fluid trapping, which causes bigger trapped boluses in the bottom half.

The number of trapped boluses rises in the top half of the channel, while it decreases in the lower half as the size of ϕ increases, as shown in Figs. 8(a) and 8(b). In fact, increasing the volume fraction of nanoparticles in the nanofluid alters its viscosity, which, in turn, affects the trapping behavior of the fluid in the asymmetric channel under peristaltic flow. This leads to an increased number of trapped boluses in the upper half and a decreased number in the lower half because peristaltic motion tries to push fluid upward because of the greater viscosity brought on by the larger volume fraction of nanoparticles. As a result, there are more trapped boluses in the upper half and less trapped boluses in the bottom portion.

Figures 8(c) and 8(d) demonstrate that, as Gr increases, more trapped boluses accumulate in both the upper and lower portions of the channel. This is due to that as the local temperature Grashof number increases, the buoyancy forces become stronger relative to viscous forces. This leads to enhanced fluid motion and mixing within the channel. Greater buoyant forces cause the fluid to be more readily moved and mixed, which leads to the formation and trapping of more boluses in the channel's upper and lower parts.

VI. CONCLUSIONS

The effects of heat transfer and Hall and ion-slip currents on the peristaltic flow of a copper–water nanofluid in an asymmetric channel are examined in this paper. Under the presumptions of a long wave length and a low Reynolds number, the problem is made simpler. The exact and closed-form solutions to the problem have been obtained. Graphs are used to describe the results. The following is a summary of the key findings:

1. With a rise in M, the base fluid velocity increases close to the channel walls and drops toward the channel's center.
2. The base fluid velocity decreased toward the channel walls and increased in the channel center when the Hall parameter was increased or copper nanoparticles were added.
3. While the axial pressure gradient reduces with an increase in d and β_e, it rises with an increase in M and ϕ.
4. With an increase in Gr, the pressure rises.
5. β_e and β_i both have the same effect on pressure rise, but ϕ has an opposite impact.
6. Adding copper nanoparticles or raising the nanoparticles volume fraction causes the base fluid's temperature to drop.
7. Increasing N_b and N_t resulted in a rise in the fluid's local temperature.
8. As N_b rises, the concentration of nanoparticles rises; however, as N_t rises, the concentration falls.
9. With an increase in M, the size of the trapped bolus reduces in the lower half of the channel and grows in the top half.
10. As β_e, ϕ, and Gr rise, the number of trapped bolus increases in the top part of the channel.

In the future, efforts could concentrate on investigating the influence of nanoparticle properties (size, shape, surface chemistry, etc.) on the peristaltic behavior of nanofluids. Understanding how these factors affect flow characteristics, heat transfer, and particle distribution can provide valuable information for optimizing nanofluid-based systems.

ACKNOWLEDGMENTS

The authors would like to extend their sincere appreciation to researchers supporting Project No. RSPD2025R1112, King Saud University, Riyadh, Saudi Arabia.

AUTHOR DECLARATIONS

Conflict of Interest

The authors have no conflicts to disclose.

Ethics Approval

The conducted research is not related to either human or animal use.

Author Contributions

All authors contributed equally and significantly to the study conception and design, material preparation, data collection and analysis. The first draft of the manuscript was written by (Kh. Nowar) and all authors commented on previous versions of the manuscript. All authors read and approved the final manuscript.

Khalid Nowar: Conceptualization (equal); Data curation (equal); Formal analysis (equal); Investigation (equal); Methodology (equal); Resources (equal); Software (equal); Validation (equal); Writing – original draft (equal). **Borhen Halouani**: Conceptualization (equal); Data curation (equal); Formal analysis (equal); Funding acquisition (equal); Supervision (equal); Validation (equal); Visualization (equal); Writing – review & editing (equal).

DATA AVAILABILITY

Data will be available on request.

NOMENCLATURE

a (m)	The traveling wave amplitude of the upper wave
a_1, a_2 (m)	Amplitudes of upper and lower waves
(a, b)	The non-dimensional amplitudes at (h_1, h_2) walls
b (m)	The traveling wave amplitude of the lower wave
$\mathbf{B}$ (wb/m^2)	Magnetic flux density
Br	The local nanoparticle Grashof number
c_1 (m/s)	Speed of peristaltic wave
C	Concentration of the fluid
C_0, C_1	Mass concentration at the top and bottom walls
d	Dimensionless width of the channel
D_B	The Brownian diffusion factor
D_T	The coefficient of thermophoretic diffusion
$\mathbf{E}$ (V/m)	The intensity of the electric field
F	The dimensionless mean flow in wave frame
g (m/s^2)	Gravitational acceleration
Gr	Local Grashof number
h_1	Dimensionless top wall
h_2	Dimensionless bottom wall
H	The dimensionless mean flow in the laboratory frame
H_1	Top wall
H_2	Bottom wall
$\mathbf{J}$ (A/m^2)	The current density
k_{eff} (w/m K)	Effective thermal conductivity
M	The Hartmann number
N_b	The Brownian motion parameter
N_t	The thermophoresis parameter
P (N/m^2)	Pressure
R_e	Reynolds number
t (s)	Time
T (K)	Temperature of fluid

T_0, T_1	Temperatures at the top and bottom walls respectively
(u, v) (m/s)	Dimensionless velocities in the moving frame of reference
(U, V) (m/s)	Velocity components in the fixed frame of reference
(x, y)	The coordinates system in the moving frame of reference
(X, Y)	The coordinates system in the fixed frame of reference
Ω	Non-dimensional concentration
β_e	The Hall parameter
β_i	The ion-slip parameter
δ	Dimensionless wave number
θ	The non-dimensionless temperature
λ (m)	The wave length
μ_{eff} (N s/m^2)	Effective viscosity
ρ_{eff} (kg/m^3)	Effective density
$(\rho c)_{eff}$ (J/kg K)	Effective specific heat
$(\rho\beta)_{eff}$ (K^{-1})	Effective thermal expansion
σ_{eff} (S/m)	Effective electric conductivity
ϕ	Nanoparticles volume fraction
Φ	The non-dimensional mass concentration
Ψ	The stream function
ω (Rad.)	The phase difference

REFERENCES

[1] S. U. S. Choi, "Enhancing thermal conductivity of fluids with nanoparticles," in *Developments and Applications of Non-Newtonian Flows*, edited by D. A. Siginer and H. P. Wang (ASME, New York, 1995), Vol. 66, pp. 99–105.

[2] K. Khanafer, K. Vafai, and M. Lightstone, "Buoyancy-driven heat transfer enhancement in a two-dimensional enclosure utilizing nanofluids," Int. J. Heat Mass Transfer **46**, 3639–3653 (2003).

[3] N. Putra, W. Roetzel, and S. K. Das, "Natural convection of nano-fluids," Heat Mass Transfer **39**(8–9), 775–784 (2003).

[4] J. Koo and C. Kleinstreuer, "Laminar nanofluid flow in microheat-sinks," Int. J. Heat Mass Transfer **48**(13), 2652–2661 (2005).

[5] J. Buongiorno, "Convective transport in nanofluids," J. Heat Transfer **128**, 240–250 (2006).

[6] M. Ghazvini and H. Shokouhmand, "Investigation of a nanofluid-cooled microchannel heat sink using Fin and porous media approaches," Energy Convers. Manage. **50**(9), 2373–2380 (2009).

[7] W. A. Khan and I. Pop, "Boundary-layer flow of a nanofluid past a stretching sheet," Int. J. Heat Mass Transfer **53**, 2477–2483 (2010).

[8] Y. M. Hung, "Analytical study on forced convection of nanofluids with viscous dissipation in microchannels," Heat Transfer Eng. **31**, 1184–1192 (2010).

[9] D. Lelea, "The performance evaluation of Al_2O_3/water nanofluid flow and heat transfer in micro-channel heat sink," Int. J. Heat Mass Transfer **54**(17–18), 3891–3899 (2011).

[10] D. Lelea and C. Nisulescu, "The micro-tube heat transfer and fluid flow of water based Al_2O_3 nanofluid with viscous dissipation," Int. Commun. Heat Mass Transfer **38**(6), 704–710 (2011).

[11] S. Asghar, Q. Hussain, T. Hayat, and F. Alsaadi, "Hall and ion slip effects on peristaltic flow and heat transfer analysis with Ohmic heating," Appl. Math. Mech. **35**(12), 1509–1524 (2014).

[12] N. S. Gad, "Effect of Hall currents on interaction of pulsatile and peristaltic transport induced flows of a particle–fluid suspension," Appl. Math. Comput. **217**, 4313–4320 (2011).

[13] E. Abo-Eldahab, E. Barakat, and Kh. Nowar, "Hall currents and heat transfer effects on peristaltic transport in a vertical asymmetric channel through a porous medium," Math. Probl. Eng. **2012**, 840203.

[14] M. Kothandapani and J. Prakash, "Effects of thermal radiation parameter and magnetic field on the peristaltic motion of Williamson nanofluids in a tapered asymmetric channel," Int. J. Heat Mass Transfer **81**, 234–245 (2015).

[15] A. M. Abd-Alla and S. M. Abo-Dahab, "Magnetic field and rotation effects on peristaltic transport of a Jeffrey fluid in an asymmetric channel," J. Magn. Magn. Mater. **374**, 680–689 (2015).

[16] S. Sharma, U. Singh, and V. K. Katiyar, "Magnetic field effect on flow parameters of blood along with magnetic particles in a cylindrical tube," J. Magn. Magn. Mater. **377**, 395–401 (2015).

[17] N. S. Akbar, "Influence of magnetic field on peristaltic flow of a Casson fluid in an asymmetric channel: Application in crude oil refinement," J. Magn. Magn. Mater. **378**, 463–468 (2015).

[18] N. S. Akbar, M. Raza, and R. Ellahi, "Influence of induced magnetic field and heat flux with the suspension of carbon nanotubes for the peristaltic flow in a permeable channel," J. Magn. Magn. Mater. **381**, 405–415 (2015).

[19] Kh. Nowar, "Effect of induced magnetic field on peristaltic transport of a nanofluid in an asymmetric channel: Closed form solution," Appl. Math. Inf. Sci. **11**(2), 373–381 (2017).

[20] F. M. Abbasi, T. Hayat, and A. Alsaedi, "Peristaltic transport of magneto-nanoparticles submerged in water: Model for drug delivery system," Physica E **68**, 123–132 (2015).

[21] N. S. Akbar, A. B. Huda, and D. Tripathi, "Thermally developing MHD peristaltic transport of nanofluids with velocity and thermal slip effects," Eur. Phys. J. Plus **131**, 332 (2016).

[22] Kh. Nowar, "Peristaltic flow of a nanofluid under the effect of Hall current and porous medium," Math. Probl. Eng. **2014**, 389581.

[23] N. S. Akbar, M. Raza, and R. Ellahi, "Peristaltic flow with thermal conductivity of H_2O + Cu nanofluid and entropy generation," Results Phys. **5**, 115–124 (2015).

[24] F. M. Abbasi, T. Hayat, and B. Ahmad, "Peristaltic transport of copper–water nanofluid saturating porous medium," Physica E **67**, 47–53 (2015).

[25] F. M. Abbasi, T. Hayat, and B. Ahmad, "Peristalsis of silver-water nanofluid in the presence of Hall and Ohmic heating effects: Applications in drug delivery," J. Mol. Liq. **207**, 248–255 (2015).

[26] H. Hassan, "Heat transfer of Cu–water nanofluid in an enclosure with a heat sink and discrete heat source," Eur. J. Mech. B **45**, 72–83 (2014).

[27] N. Iftikhar, A. Rehman, H. Sadaf, and M. Najam Khan, "Impact of wall properties on the peristaltic flow of Cu-water nano fluid in a non-uniform inclined tube," Int. J. Heat Mass Transfer **125**, 772–779 (2018).

[28] F. M. Abbasi, T. Hayat, B. Ahmad, and G. Q. Chen, "Slip effects on mixed convective peristaltic transport of copper-water nanofluid in an inclined channel," PLoS One **9**(8), e105440 (2014).

[29] S. Das, B. Barman, and R. N. Jana, "Influence of Hall and ion-slip currents on peristaltic transport of magneto-nanofluid in an asymmetric channel," BioNanoScience **11**, 720–738 (2021).

[30] S. Das, B. Barman, and R. N. Jana, "Hall and ion-slip currents' role in transportation dynamics of ionic Casson hybrid nano-liquid in a microchannel via electroosmosis and peristalsis," Korea-Aust. Rheol. J. **33**(4), 367–391 (2021).

[31] M. Rafiq, H. Yasmin, T. Hayat, and F. Alsaadi, "Effect of Hall and ion-slip on the peristaltic transport of nanofluid: A biomedical application," Chin. J. Phys. **60**, 208–227 (2019).